Anal. Methods Environ. Chem. J. 7 (3) (2024) 99-112

AMECJ

Research Article, Issue 3
Analytical Methods in Environmental Chemistry Journal
Journal home page: www.amecj.com/ir

Simultaneous transmittance and fluorescence excitation-emission matrix spectroscopy coupled to multivariate analysis for the determination of Galaxolide in surface water samples

Thomas Ingwani[a], Nhamo Chaukura[b,*], Bhekie B. Mamba[a], Thabo T.I. Nkambule[a], and Adam M. Gilmore[a,c]

[a]*Institute for Nanotechnology and Water Sustainability, College of Engineering, Science and Technology, University of South Africa, Johannesburg,1709, South Africa*

[b]*Department of Physical and Earth Sciences, Sol Plaatje University, Kimberley, 8300, South Africa*

[c]*Horiba Instruments Incorporated, Piscataway, New Jersey, 08854, USA.*

ARTICLE INFO:

Received 26 May 2024
Revised form 30 Jul 2024
Accepted 27 Aug 2024
Available online 29 Sep 2024

Keywords:
Fluorescence excitation-emission matrices spectroscopy,
Absorbance-transmittance spectroscopy,
Galaxolide,
Surface water,
Multivariate analysis,
Analytical method

ABSTRACT

Recently, emerging micropollutants have gained significant attention from researchers and the general public due to their expanding distribution in the environment and mostly unknown effects on human and environmental health. To detect and quantify Galaxolide (HHCB) in surface water, we used simultaneous absorbance-transmittance and fluorescence excitation-emission matrices (A-TEEM) spectroscopy in conjunction with partial least squares (PLS) and parallel factor (PARAFAC) analyses. The fluorescence spectra of surface water samples laced with HHCB standard solutions were obtained using an A-TEEM spectrometer. The PARAFAC analysis of the fluorescence spectra revealed four fluorescent organic matter components; among them, the HHCB spiked into the samples. Regression analysis of the measured versus predicted concentrations showed a high correlation coefficient of calibration (0.966), high Pearson r value (0.999), good root mean square of prediction error divided by the standard deviation (1.715), and a low ratio of range error (14.286). The results of the A-TEEM-PLS technique under optimized and validated conditions were as follows: a low limit of detection (LLOD:4.01×10^{-8} M), a reasonably wide working range (WWR: 1.16 × 10^{-8} - 1.16 ×10^{-6} M), a narrow mean relative standard deviation (MRSD: 0.198 %), and a high recovery (R: 101%). These findings demonstrate the importance of using the straightforward and effective A-TEEM-PLS method to detect and monitor this ubiquitous environmental material in aquatic systems.

1. Introduction

Galaxolide, hexahydro-4,6,6,7,8, hexamethyl cyclopenta[g]benzopyran (HHCB), is a synthetic polycyclic musk that is used as a fragrance component in an assortment of personal care products, including cosmetics, perfumes, shampoos, detergents, lotions, fabric softeners, and cleaning agents (Fig.1). Because of its extensive usage in personal care products, HHCB is commonly found in aquatic systems [1,2]. The chemical structure of HHCB renders it recalcitrant to hydrolysis under environmental conditions; hence, it will persist in aquatic systems. Given that HHCB is toxic to marine life and humans, studies into its prevalence, toxicity, characterization, and treatment have recently attracted considerable attention [3,4]. Human exposure pathways include

*Corresponding Author: Nhamo Chaukura
Email: nhamo.chaukura@spu.ac.za
https://doi.org/10.24200/amecj.v7.i03.322

the skin, lungs, and gastrointestinal tract. Due to the capacity to interfere with hormonal function in humans [5,6], HHCB has been assigned a moderate risk to human health. Many ailments related to metabolism, behavior, reproduction, and development are linked to hormone disruption. Consequently, the U.S. Environmental Protection Agency (EPA) classified HHCB as a high-priority substance [7,8]. Therefore, extracting, characterizing, and removing HHCB from environmental water sources is crucial. Therefore, simple, reasonably priced techniques are crucial for identifying HHCB in aquatic settings. The occurrence of HHCB has been reported in various aquatics systems worldwide. For example, surface waters in Canada, Sweden, the USA, Korea, China, and Austria have high HHCB concentrations of as high as 1.017×10^{-7} M [9-11]. In South Africa, water samples from Gauteng, the North West, and Mpumalanga Provinces had high HHCB concentrations (1.361×10^{-5} M) [12,6]. With the aid of a light beam, electrons of certain compounds are excited and, upon relaxation, release light in the process of fluorescence [13,14]. Fluorometry, or fluorescence spectroscopy, is an instrumental method of analyzing the light emitted. For HHCB determination, an aqueous solution containing HHCB is scanned on a simultaneous absorbance-transmittance and excitation-emission matrices (A-TEEM) spectrometer. By concurrently acquiring the three-dimensional (3-D) excitation-emission matrices and the absorbance spectra, the effects of inner filters are removed, allowing for accurate interpretation of the data [15] and minimization of variations resulting from sample conditions or geometry [16]. The fluorescence spectral data are then interpreted using chemometric algorithms, for example, partial least squares (PLS), extreme gradient boosting (XGB), artificial neural networks, and parallel factor (PARAFAC) analyses. The versatility of the A-TEEM method, in conjunction with multi-way analysis, allows the examination of various organic materials. Hence, this method presents a water quality monitoring tool that is quick, nearly real-time, sensitive, user-friendly, cost-effective, reagent-free, and extraction-free [17]. A-TEEM spectroscopy has been used in several analyses, including the characterization of aromatic petroleum hydrocarbons or oils, polycyclic aromatic hydrocarbons [18], dyes [19], monitoring micropollutants [17] membrane integrity [20], and monitoring extracellular polymeric materials [21]. Multivariate analysis provides a more thorough analysis of the data by examining every potential independent variable and how they might relate to each other. This, consequently, assists in making decisions about procedures, forecasting future results, and fixing errors. The cause-and-effect relationships between variables can be determined, and large data sets can be analyzed. The main analytical techniques for the analysis of HHCB include high-performance liquid chromatography (HPLC) and gas chromatography in tandem with mass spectrometry (GC/MS) [22-24]. This is after sample treatment using solid-phase microextraction [24] and photolytic breakdown [25]. Some of the benefits of GC/MS over alternative techniques include high separation efficiency, identification of isomers, instrument accessibility, reproducibility, sensitivity, robustness, low cost, and ease of use [26-28]. Herein, A-TEEM-PARAFAC and A-TEEM-PLS techniques for identifying and quantifying HHCB in surface water samples, respectively, at trace levels were developed, optimized, and validated for analyzing surface water samples laced with HHCB following some International Conference on Harmonization [29], United States Pharmacopeia [30], and American Society for Testing and Materials [31], recommendations and meeting requirements for acceptance. The EEM data acquired using the A-TEEM were analyzed using optimized three-way PARAFAC and PLS models. The qualitative analysis model for HHCB and fluorophores in surface water was established using PARAFAC modeling. Then, the categorization of fluorophores in HHCB-spiked surface water was performed based on previous studies. The model for quantitative analysis of HHCB was developed by applying PLS modeling, and then the concentration of HHCB in the validation sets was determined. Excellent and relevant statistical results were obtained to quantify HHCB in surface water.

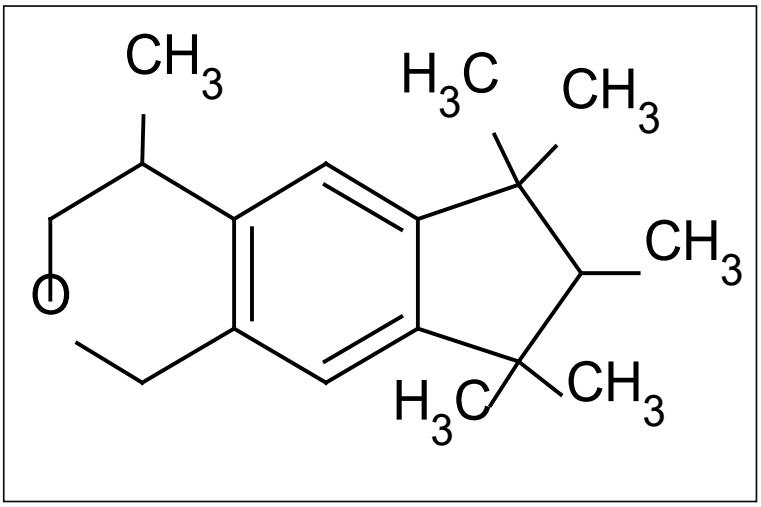

Fig. 1. Galaxolide chemical structure

2. Experimental

2.1. Materials and reagents

Analytical grade (AG) of methanol (CAS Number: 67-56-1) and HHCB (CAS Number: 1222-05-5) with a purity grade of 99%, and 0.45 micron glass microfiber (GMF) filters were purchased from Sigma-Aldrich® (Johannesburg, South Africa). Deionized water was produced using an Elix Integral 10 filter for water from Merck Millipore (South Africa).

2.2. Sampling

The Florida stream in Johannesburg, Gauteng, South Africa (26.1739° S, 27.8971° E) was the source of grab water samples taken on January 31, 2023, in one liter of clean amber glass bottles [32]. The samples were then kept at 4°C before being spiked with HHCB, and their fluorescence characteristics were examined. Subsequently, the samples were allowed to warm to room temperature, filtered through 0.45 micron GMF filters, and spiked with known concentrations of HHCB.

2.3. Preparation of a stock solution and an intermediate standard solution

A 100 mL volumetric flask containing 0.102 g of 99% pure HHCB was weighed using a Mettler Toledo analytical balance (Greifensee, Switzerland). This was dissolved in methanol and then topped to the mark to produce a 3.87×10^{-3} M stock solution. In a 100 mL volumetric flask, 0.1 mL of the stock solution was diluted to the mark with AG methanol to give a 3.87×10^{-6} M intermediate standard solution.

2.4. General procedure

2.4.1. Titration method for calibration

Aliquots of filtered surface water samples and intermediate HHCB standard solutions were placed in the same quartz cuvette to obtain 100 calibration standards with concentrations within the 1.16×10^{-8} to 1.16×10^{-6} M range and 20 validation samples with HHCB concentrations within the 5.8 10^{-8} to 1.16×10^{-6} M range. On completion, the cuvette had a total volume of 4000 µL. After that, the cuvette was vigorously shaken to homogenize the sample. To rule out the possibility of methanol altering the solution's refractive index or creating a luminous background, less than 2% of the final methanol concentration in the cuvette was maintained [33].

2.4.2. Instrumental and software

Absorbance spectra and EEM data were collected from surface water samples that had been spiked with HHCB-standard solutions and samples that had not, using the Aqualog® spectrometer (HORIBA Yobin Yvon model UV-800C, New Jersey, USA). The instrument was set at a fixed optical slit width of 5 nm, emission wavelengths between 245.21 and 827.32 nm separated by 8 pixels (4.66 nm),

and excitation wavelengths between 200 and 800 nm separated by 5 nm. Data from the EEM were gathered using the sample queue technique, and the EEM spectra were used as fluorescent signatures.

2.4.3. PARAFAC modeling

The 120 EEM dataset was modeled using PARAFAC via Eigenvector Solo software (version 8.7). Inner filter effects, primary and secondary Raman scatter, and artifactual first- and second-order Rayleigh scatter were all corrected using customized spectrometer software functions [34]. For EEM filtering, the first-order Rayleigh filter was set to 16 nm and the second-order Rayleigh filter to 32 nm. The default Raman shift of 3382 cm^{-1} and a filter half-width of 16 nm were used to eliminate Raman scattering. The Ex/Em 350/396.5 nm 2D-spectrum of a sealed water-Raman cuvette was measured and used to normalize the corrected EEM into Raman units. The bandwidth was adjusted to avoid fluorescence peaks crossing over or getting too close to the Rayleigh or Raman scatter. A PARAFAC model must be fitted with the correct number of components for the chemical interpretation to be valid. Models with one to five components were validated using split-half analysis, spectral loadings, the core consistency diagnostic, and the percent captured variance.

2.4.4. PLS modeling

A calibration model was built using 100 EEM spectra from the calibration set, and a validation model was tested using 20 EEM spectra. This allowed for the analysis of the concentration of HHCB validation samples. Eigenvector Solo software suite version 8.6 was used to perform the PLS analysis program for model building and validation. PLS modeling compared the variables in the EEM data to variables in the HHCB concentration. When using the Solo software suite, the PLS workflow has three primary phases: (1) *EEM data importation*: Mean-centering is used to preprocess the data after they have been imported. Beginning with the one with the most minor partial correlation with the EEM data variable, each HHCB concentration variable is gradually removed from the equation. The process is terminated when none of the equation's variables satisfies the elimination requirements. In this work, latent variables (LVs) were chosen; (2) *EEM data splitting*: A total of 120 EEM data points were manually divided into two datasets: a validation dataset (20 data points) and a calibration dataset (100 data points); and (3) *Iterations*: Cross-validation is repeated until the lowest root mean square error for cross-validation (RMSECV) and highest R^2 values are obtained. A preprocessing step was not performed on the spectral (X-block) calibration dataset. After mean-centering and autoscaling [35], the concentration calibration (Y-block) data were preprocessed. The calibration, cross-validation, and prediction correlation coefficients were used to assess the efficacy of the regression model. Based on the parameters of the generated error matrix, the data were classified using the strict ($p > 0.5$) and most likely rules of the total number of positive identifications. The quality of the model was assessed by evaluating several PLS model performance parameters derived from PLS analyses of the EEM data from surface water samples spiked with HHCB standard solutions at concentrations ranging from 1.16×10^{-8} to 1.16×10^{-6} M. The parameters included the number of LVs, the slope of the calibration curve, the correlation coefficients for calibration (R^2 Cal), cross-validation (R^2 CV), and prediction (R^2 Pred), bias in the calibration and prediction processes, and root mean square errors for calibration (RMSEC), prediction (RMSEP), and RMSECV.

2.5. Validation of spiked samples

Origin version 8.6 was used to regress further the data obtained from the PLS analysis of the validation samples. A regular residual versus the HHCB concentration plot and a predicted and measured HHCB concentration plot were generated. The regression parameters were generated using the predicted and measured HHCB concentration plot, and they were then combined with other goodness-of-fit parameters to create a linear regression report. The regression parameters included slope, standard

error of the slope, intercept, and adj. R^2, Pearson r value, residual sum of squares, and intercept standard error. Plotting the regular residual against the HHCB concentration provides the residual distribution. The statistical parameters for the degrees of freedom, sum of squares, mean squares, F-value, and Prob > F or p-value were obtained in an ANOVA table. The F value was used to determine the statistical significance of the analysis at p-value (Prob > F). The relationship between the predicted and measured HHCB concentration variables was determined by calculating the p-value (Prob > F value), which was used to evaluate the null hypothesis, which claims that there is no relationship between any of the measured or predicted HHCB concentrations [36].

2.5.1.Limits of quantitation and detection

Based on the slope and intercept of the calibration curve as well as the intercept standard error, the limits of detection (LOD) and limits of quantitation (LOQ) of HHCB were calculated and showed in Equations 1 and Equations 2, respectively [33]. Table 1 of the report on linear regression analysis contains the appropriate linear regression parameters used to compute the LOD and LOQ.

$$LOD = 3 \times \frac{Standard\ error\ of\ intercept + Intercept}{Slope\ of\ calibration\ curve} \quad \text{(Eq.1)}$$

$$LOQ = 10 \times \frac{Standard\ error\ of\ intercept + Intercept}{Slope\ of\ calibration\ curve} \quad \text{(Eq.2)}$$

2.5.2.Method recovery

Three concentrations of HHCB standards were spiked into blank surface water samples. These were (1) close to the highest possible quantitation (high), (2) close to the middle of the calibration range (medium), and (3) close to the quantification point (low). After that, the fluorescence spectra of the samples were obtained to evaluate the validity of the recovery method. The calibration spectra were acquired similarly to the spectra of the validation samples to provide accurate results. The percentage recovery (Equation 3) was computed at three HHCB concentrations (1.16×10^{-8}, 3.503×10^{-7}, and 1.16×10^{-6} M) [37]:

$$\%Recovery = \frac{obtained\ result}{expected\ result} \times 100 \quad \text{(Eq.3)}$$

Previous studies show that the recommended range for the mean recovery is between 70% and 120% [38]. Based on the outcomes, compliance with these recommendations was evaluated. The concentrations of HHCB in three surface water samples spiked with HHCB standard solutions at concentrations of 1.16 10^{-8}, 3.503 10^{-7}, and 1.16 10^{-6} M were measured four times each using the A-TEEM-PLS technique. The relative standard deviation (%RSD) was calculated as Equation 4 [39]. The %RSD must be at least 2% as the acceptance criterion [40].

$$\%RSD = \frac{standard\ deviation}{mean} \times 100 \quad \text{(Eq.4)}$$

3. Results and discussion

3.1. Fingerprint of the excitation-emission matrix of HHCB

We compared the two-dimensional (2-D) fluorescence spectra of two surface water samples one spiked with HHCB and the other not spiked with HHCB (Fig. 2). Figure 2a shows the EEM of fluorescent organic matter in a neat (baseline or blank) surface water sample. In the neat surface water sample, it was discovered that the fluorophores showed wavelengths of 230–425 nm for excitation and 325–600 nm for emission, suggesting the presence of humic substances [RS 41, RS42]. Figure 2b shows the molecular fingerprint of the EEM of HHCB in a surface water sample that was spiked with 8.13×10^{-8} M of HHCB. This figure shows that the wavelengths at which HHCB was found to excite and emit were ~275 and ~296 nm, respectively.

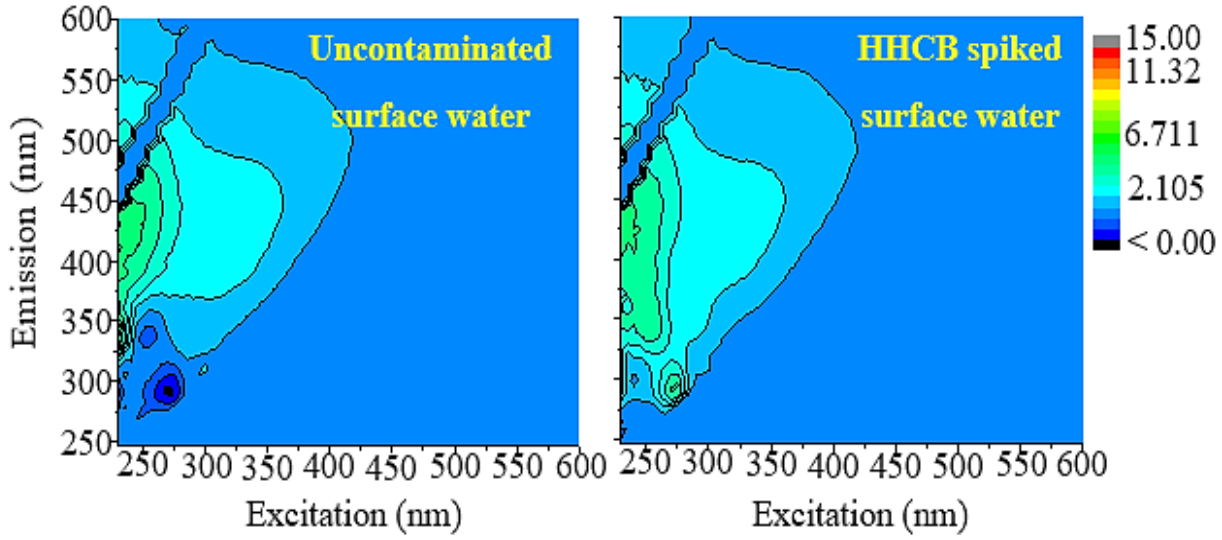

Fig. 2. The 2-D EEMs of two samples of surface water: **(a)** one that is unspiked (DOC = 1.73 ppm) and **(b)** HHCB (1.74×10^{-7} molL^{-1}) spiked in surface water

3.2. PARAFAC modeling and validation

Four components were the ideal number because the explained variance, split-half similarity evaluation, core consistency, spectral loadings, and component identification were balanced. Figure 3 shows the 2-D contour maps of EEMs for the four fluorophores identified in surface water samples spiked with HHCB, as determined by PARAFAC. The categorization of the PARAFAC components shown in this figure was performed after a review of the literature. Component #1, which had maximum wavelengths of ~270 and ~300 nm, respectively, for excitation and emission, represented HHCB (Fig. 3a). This component's Ex/Em wavelength pair almost agreed with those used for fluorescence detection of HHCB in a previous study [25]. The second, third, and fourth components represented organic substances that resembled tryptophan (Fig. 3c) [RS43], fulvic acid (Fig. 3e), and humic acid (Fig. 3g) [RS44] with maximum excitation and emission wavelengths of, respectively, ~ 390 and 450 nm [RS45], 240 to 320 nm and ~ 450 nm, and ~ 390 and 450 nm [RS46]. Furthermore, the spectral loading plots for emission and excitation wavelengths produced by PARAFAC modeling of the EEM data are shown in Figures 3b, 3d, 3f, and 3h. These plots correspond with the wavelengths at which the 2-D contour plots of the emission and excitation of the four components are depicted.

3.3. PLS modeling and validation

Figure 4 displays the fluorescence spectra for 120 HHCB-spiked samples of surface water (Figure 4a) [RS47]., as well as the evolution of the RMSECV, represented by a blue line, and the fundamental RMSEC, represented by a green line, depending on the number of latent LVs used to construct the PLS HHCB prediction model (Figure 4b). Upon analyzing the peaks visually, a single area exhibiting a maximum emission wavelength of ~296 nm was identified and is shown in Figure 4a. A minimum of 5 LVs is shown (Figure 4b) [RS48].

Plots of samples and scores were created to locate and ostensibly eliminate outliers (Fig. 5) [RS49]. The measured and predicted HHCB concentrations using the 120 EEM spectra show a strong correlation, with a high R^2 Cal value of 0.966 in Figure 5a. The plot of scores on LV2 and LV1 indicated six outliers (Fig. 5b). There were a significant number of outliers on the plot that were outside the 95% confidence intervals (blue dashed lines), according to the Q residuals reduced versus the T^2 statistic of the Hotelling plot (Fig. 5c). Four observations with high leverage in the middle and left of the plot shown in Figure S2d were noted. All outliers were eliminated because they can skew statistical analyses [RS50].

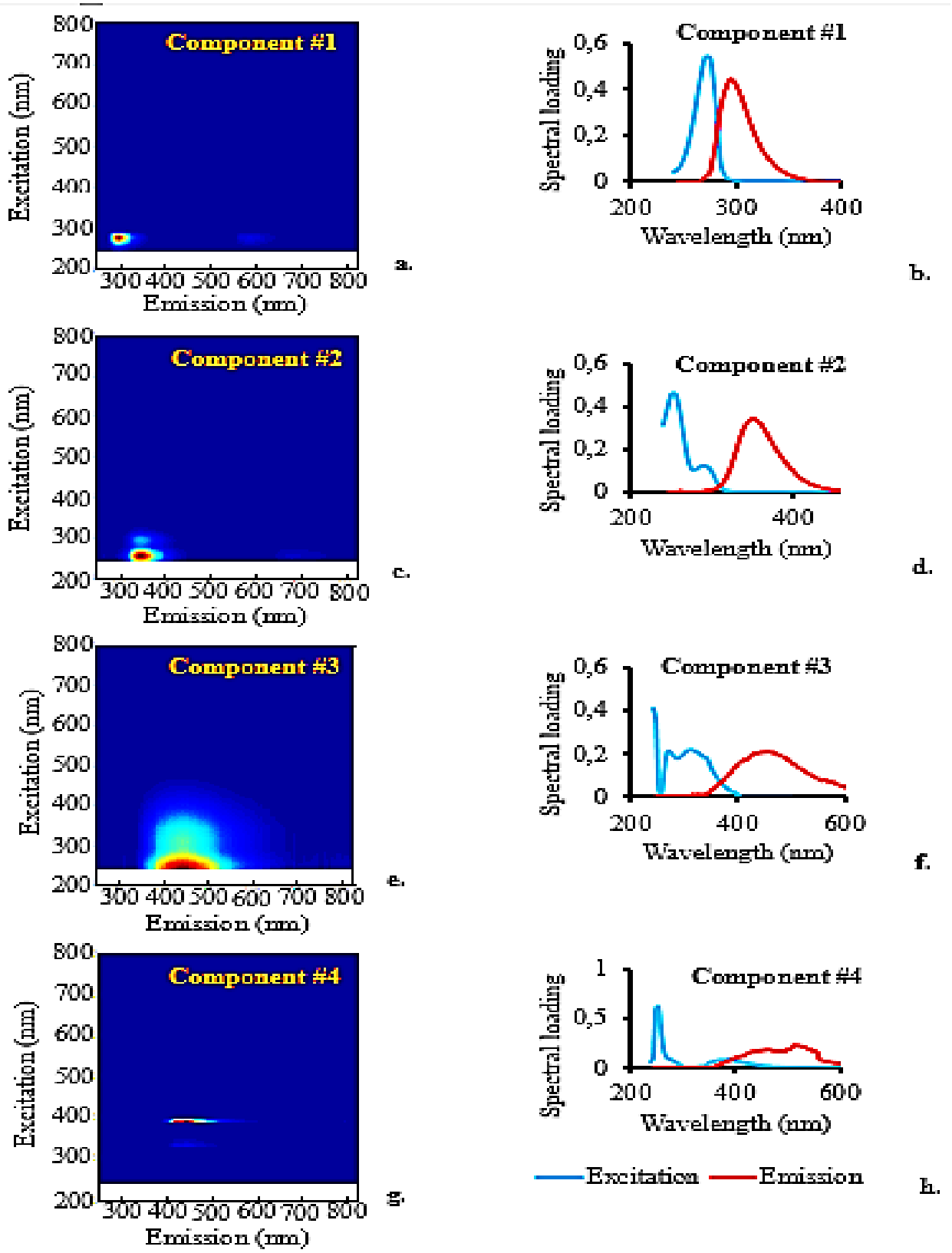

Fig. 3. Four-constituent PARAFAC model: 2-D EEM maps and spectral loadings for excitation and emission of the four constituents of the HHCB-spiked surface water spectral dataset. Components #1, #2, #3, and #4 represent, HHCB, organic material resembling tryptophan acid, organic material resembling fulvic acid, and organic material resembling humic acid.

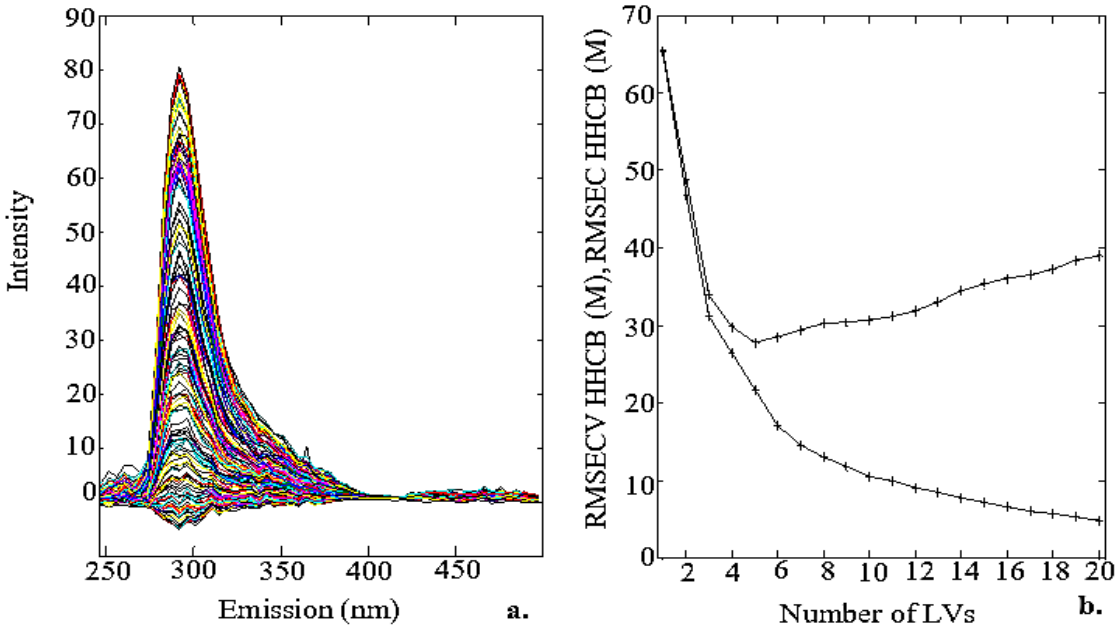

Figure 4 (a) Emission spectra for 120 surface water samples that were spiked with HHCB standard solutions at concentrations between 1.16×10^{-8} and 1.16×10^{-6} M.
(b) Development of the RMSECV (blue line) and the basic RMSEC (green line) per the number of LVs used to build the PLS HHCB prediction model. A minimum of 5 LVs is shown.

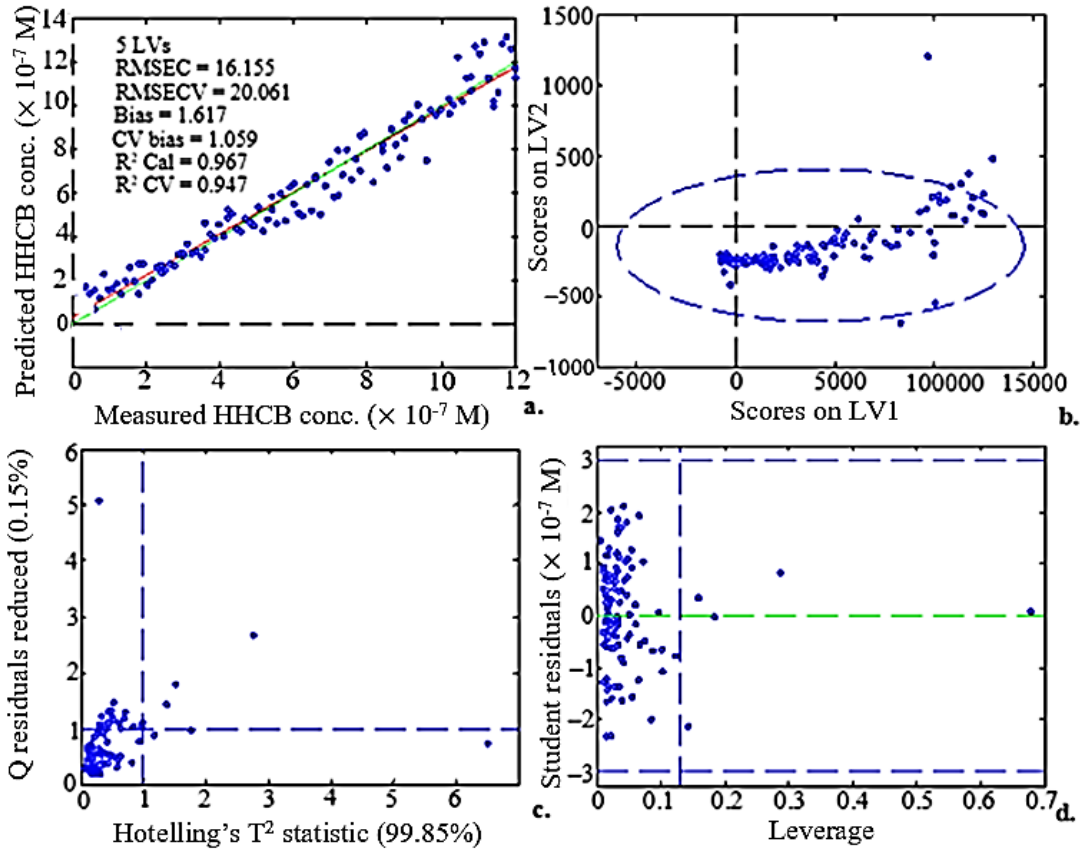

Fig. 5. Plots of **(a)** predicted versus measured HHCB concentration (M), **(b)** scores on LV2 versus scores on LV1, **(c)** Q residuals reduced versus Hotelling's T^2 statistic, and **(d)** studentized residuals HHCB (M) versus leverage for the HHCB concentration range (1.16×10^{-8} and 1.16×10^{-6} M)

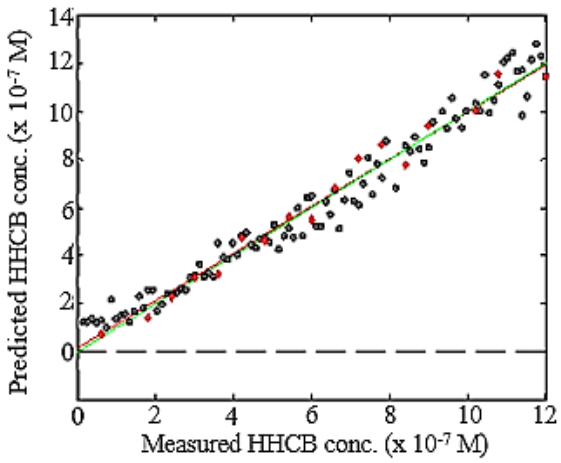

Table 1. The linear regression analysis report for the analysis of HHCB (From Origin V8.6)

Parameter	Value
Number of LVs	5
% Variance captured	95.42
RMSECV (M)	8.058 × 10-8
RMSEC (M)	6.3 × 10-8
RMSEP (M)	5.613 × 10-8
R2 (Cal, CV)	0.966, 0.944
R2 Pred	0.976
RPD (RMSECV, RMSEP)	1.715, 1.187
Slope of calibration curve	1.00
Prediction Bias	–0.623
Calibration Bias	1.554
CV Bias	1.036

Fig. 6. A graph of the measured HHCB concentration (M) against the predicted one for a validation dataset consisting of 18 data points (shown as red diamonds) and a calibration dataset composed of 100 data points (shown as black dots) along with the performance metrics of the PLS model for the examination of HHCB-spiked surface water are shown. LVs is an abbreviation of latent variables, RMSEC means calibration root mean square error, RMSECV means cross-validation accuracy root mean square error, RMSEP means root mean square error of prediction, R^2 (Cal, CV) means calibration and cross-validation accuracy correlation coefficients, R^2 Pred stands for the prediction accuracy correlation coefficient, and CV bias is bias brought on by the coefficient of variation.

Figure 6 shows the calibration and validation of HHCB concentration curves after dividing 120 HHCB EEM spectra into two sets of data: a validation set of 20 data points (red diamonds) and a calibration set of 100 data points (black dots). According to the performance parameters, all validation samples for the PLS model demonstrated accuracy and dependability. There was a value of 6.3 × 10-8 M in the calibration set, and 8.058 × 10-8 M was found in the validation set for the RMSECV. These results implied excellent robustness and predictive accuracy of the PLS model [51].

3.4. Spike sample validation results

The measured versus predicted HHCB concentration plot shows 95% confidence and prediction intervals (Fig. 7a). It is necessary to compute the confidence interval for each potential value of the independent variable. Figure 7b shows the regular residual versus the HHCB concentration plot. The linear regression model successfully predicted the data, as demonstrated by the regular residuals of ±7.74 × 10^{-8} M and the randomly distributed points on the residual plot along the horizontal axis [52].

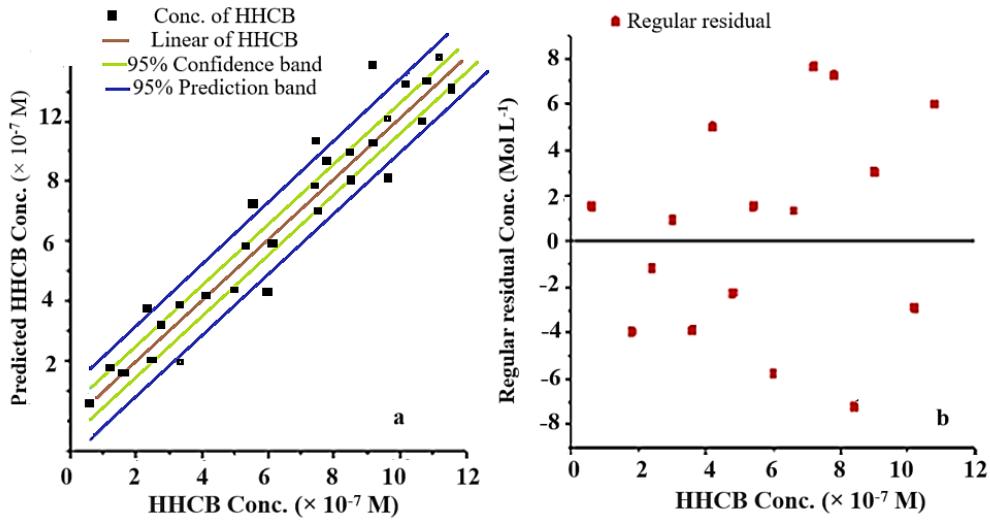

Fig. 7. **(a)** The linear fit of the data from the HHCB validation.
(b) The HHCB regular residuals against the HHBC concentration graph Mol L^{-1}

3.5. Statistical evaluation

The linear regression parameters are shown in Table 2. The small residual sum of squares in the linear regression analysis of HHCB concentrations suggests that the PLS model adequately fits the data [RS53]. The small intercept standard error value for the HHCB regression analyses (Table 2) proved that the analytical approach was valid [RS54]. The predicted HHCB concentration could account for 98.0% of the variation in the measured HHCB concentration, according to the linear fit with R^2 = 0.98.

Furthermore, a highly significant F value of 775.325 [RS55] indicates that the model correctly predicted the HHCB concentration. The Prob > F (p-value) of $5.551E^{-15}$ (Table 3) showed significant goodness of fit between the model and data, further supporting the significance of the analytical method from a statistical standpoint [RS56]. The p-value, which was less than 0.05, meant that the null hypothesis according to which there should be no relationship between any of the predicted HHCB concentrations and the measured HHCB concentrations was not accepted [RS57].

3.6. Detection and quantitation thresholds

The lowest concentration of HHCB in surface water that the suggested method could reliably detect was 5.9×10^{-8} M, and the lowest concentration of HHCB that the technique could quantify while still maintaining the required levels of precision, accuracy, and uncertainty was 1.97×10^{-7} M.

3.7. Recovery of the proposed technique

As per the UNODC [RS58] and BioPharma international [RS59] guidelines, Table 4 presents the percentage recoveries of the method at the three concentration levels. The average recovery results, which came in at 101.12% of the predicted value, demonstrated the method's accuracy.

Table 2. The linear regression analysis report for the analysis of HHCB (From Origin V8.6)

Parameter	Value
Residual sum of squares	2352.03
R-Square (COD)	0.98
Adj. R-Squared	0.979
Pearson's r value	0.99
Intercept	1.288
Standard error of the intercept	6.464
Slope	1.086
Standard error of the slope	0.019

Table 3. ANOVA table for linearity of the HHCB regression model

ANOVA	Mean Squares	Sum of Squares	Prob > F	F Value	Degrees of Freedom
Model	-------	113974.198	$5.551E^{-15}$	775.325	0
Error	147.002	2352.03	-------	-------	16
Total	-------	116326.228	-------	-------	16

Table 4. Percentages of HHCB recovered from surface water samples spiked at three distinct concentration levels

Measured HHCB conc. (mol L^{-1})	Predicted HHCB conc. (mol L^{-1})	Recovery (%)
$1.161\ 10^{-8}$	$1.17\ 10^{-8}$	100.78
$3.503\ 10^{-7}$	$3.572\ 10^{-7}$	101.97
$1.161\ 10^{-6}$	$1.168\ 10^{-6}$	100.6

3.8. Relative standard deviation

HHCB concentrations typically had low % RSD during replicate measurement concentration. The fact that these RSD values are less than the acceptance threshold of 2.0% indicates the procedure for determining the HHCB concentration was accurate and consistent [40 and RS60]. The %RSD values of 0.195, 0.149, and 0.249 at HHCB concentrations of 1.106×10^{-8}, 3.513×10^{-7}, and 1.106×10^{-6} M, respectively, showed the effectiveness of the A-TEEM-PLS approach for HHCB analysis in surface water.

4. Conclusion

Using the fluorescence EEM data along with the PLS and PARAFAC chemometric modeling, it was possible to identify and measure HHCB in surface-level water. The fluorescence EEM data from surface water laced with HHCB allowed the two chemometric models to produce much more focused information. The HHCB could be detected by acquiring the fluorescence EEM contour plots and PARAFAC modeling of these. The maximum excitation and emission wavelengths for HHCB in surface water were ~ 270 and 296 nm, respectively. PLS modeling of fluorescence EEMs with detection and quantification limits in the lower parts per billion range can be used to predict HHCB concentrations in water. The following parameters defined the optimized and validated A-TEEM-PLS technique: working range (1.16×10^{-8} to 1.16×10^{-6} M) recovery (101%), mean relative standard deviation (0.198%), LOD (4.01×10^{-8} M), and LOQ (1.203×10^{-7} M). Using extraction- and reagent-free methods for fluorescence measurement of water contaminated with HHCB has allowed the development of a simple-to-use, cost-effective, sensitive, and rapid approach to measuring HHCB at minute amounts in water samples. Only surface water filtration is required. Thus, environmental monitoring can be conducted regularly using the suggested methodology, especially in areas where HHCB is more pronounced.

5. Acknowledgements

We are grateful to Dr. W. Moyo for the assistance in operating the Aqualog® spectrometer and Mr. S. Mhlongo for general assistance. This work was funded by the Institute for Nanotechnology and Water Sustainability at the University of South Africa. All writers have no competing interests, either monetary-related or not.

6. References

[1] H. P. Hutter, P. Wallner, W. Hartl, M. Uhl, G. Lorbeer, R. Gminski, V. Mersch-Sundermann, M. Kundi, Higher blood concentrations of synthetic musks in women above fifty years than in younger women, Int. J. Hyg. Environ. Health, 213 (2010) 124–130. https://doi.org/10.1016/j.ijheh.2009.12.002

[2] S. Teimoori, A. H. Hassani, M. Panahi, N. Mansouri, Rapid extraction of BTEX in water and milk samples based on functionalized multi-walled carbon nanotubes by dispersive homogenized-micro-solid phase extraction, Food Chem., 421 (2023) 136229. https://doi.org/10.1016/j.foodchem.2023.136229

[3] K. Vimalkumar, N. P. Nikhil, E. Arun, M. Mayilsamy, R. Babu-Rajendran, Synthetic musks in surface water and fish from the rivers in India: Seasonal distribution and toxicological risk assessment, J. Hazard. Mater., 414 (2021) 1–10. https://doi.org/10.1016/j.jhazmat.2021.125558

[4] J. H. Hong, J. Y. Lee, H. J. Ha, J. H. Lee, S. R. Oh, Y. M. Lee, M. Y. Lee, K. D. Zoh, Occurrence and sources of synthetic musk fragrances in the sewage treatment plants and the Han River, Korea, Water, 13 (2021) 1–14. https://doi.org/10.3390/w13040392

[5] D. B. Simmons, V. L. Marlatt, V. L. Trudeau, J. P. Sherry, C. D. Metcalfe, Interaction of Galaxolide with the human and trout estrogen receptor-α, Sci. Total Environ., 408 (2010) 6158–64. https://doi.org/10.1016/j.scitotenv.2010.09.027

[6] S. Teimoori, An immobilization of aminopropyl trimethoxysilane-phenanthrene carbaldehyde on graphene oxide for toluene extraction and separation in water samples, Chemosphere, 316 (2023) 137800. https://doi.org/10.1016/j.chemosphere.2023.137800

[7] EPA, Final Scope of the Risk Evaluation for 1, 3, 4, 6, 7, 8 - Hexahydro - 4, 6, 6, 7, 8, 8 - Hexamethylcyclopenta [γ] - 2 - Benzopyran. Office of Chemical Safety and Environmental Protection Agency Pollution Prevention, Washington, DC, (2020). https://www.epa.gov/assessing - and - managing - chemicals-under-tsca/risk - evaluation - 134678 - hexahydro - 466788

[8] J. Rakhtshah, A rapid extraction of toxic styrene from water and wastewater samples based on hydroxyethyl methylimidazolium tetrafluoroborate immobilized on MWCNTs by ultra-assisted dispersive cyclic conjugation-micro-solid phase extraction, Microchem. J., 170 (2021) 106759. https://doi.org/10.1016/j.microc.2021.106759

[9] K. M. Blum, P. L. Andersson, L. Ahrens, K. Wiberg, P. Haglund, Persistence, mobility and bioavailability of emerging organic contaminants discharged from sewage treatment plants, Sci. Total Environ., 612 (2018) 1532–1542. https://doi.org/10.1016/j.scitotenv.2017.09.006

[10] F. Wong, M. Robson, L. Melymuk, C. Shunthirasingham, N. Alexandrou, M. Shoeib, E. Luk, P. Helm, L. Diamond Miriam, H. Hung, Urban sources of synthetic musk compounds to the environment, Environ. Sci.: Process. Impacts, 21 (2019) 74–88. https://doi.org/10.1039/C8EM00341F

[11] M. Clara, O. Gans, G. Windhofer, U. Krenn, W. Hartl, K. Braun, S. Scharf, C. Scheffknecht, Occurrence of polycyclic musks in wastewater and receiving water bodies and fate during wastewater treatment, Chemosphere, 82 (2011) 1116–1123. https://doi.org/10.1016/j.chemosphere.2010.11.041

[12] E. M. Wanda, B. B. Mamba, T. A. Msagati, Hydrochemical modelling of water quality in terms of emerging micropollutants in Mpumalanga, Gauteng and North West Provinces, Phys. Chem. Earth. Parts A/B/C, 100 (2017) 143–57. https://doi.org/10.1016/j.pce.2016.12.004

[13] H. Itagaki, Fluorescence spectroscopy, Experimental Methods in Polymer Science, Academic Press, San Diego, CA, pages155-260, 2000. https://doi.org/10.1016/B978-0-08-050612-8.50009-X

[14] R. Ashouri, Dynamic and static removal of benzene from air based on task-specific ionic liquid coated on MWCNTs by sorbent tube-headspace solid-phase extraction procedure, Int. J. Environ. Sci. Technol., 18 (2021) 2377-2390. https://doi.org/10.1007/s13762-020-02995-4

[15] D. N. Kothawala, K. R. Murphy, C. A. Stedmon, G. A. Weyhenmeyer, L. J. Tranvik, Inner filter correction of dissolved organic matter fluorescence, Limnol. Oceanogr.: Meth., 11 (2013) 616–630. https://doi.org/10.4319/lom.2013.11.616

[16] A. Quatela, A. M. Gilmore, K. E. Gall, M. Sandros, K. Csatorday, A. Siemiarczuk, B. B. Yang, L. Camenen, A-TEEM, a new molecular fingerprinting technique: Simultaneous absorbance-transmission and fluorescence excitation-emission matrix method, Methods Appl. Fluoresc., 6 (2018) p.027002. https://doi.org/10.1088/2050-6120/aaa818

[17] M. Park, S. A. Snyder, Sample handling and data processing for fluorescent excitation-emission matrix (EEM) of dissolved organic matter (DOM), Chemosphere, 193 (2018) 530–537. https://doi.org/10.1016/j.chemosphere.2017.11.069

[18] A. K. Driskill, J. Alvey, A. D. Dotson, P. L. Tomco, Monitoring polycyclic aromatic hydrocarbon (PAH) attenuation in Arctic waters using fluorescence spectroscopy, Cold Reg. Sci. Technol., 145 (2018) 76–85. https://doi.org/10.1016/j.coldregions.2017.09.014

[19] M. A. Pendergraft, D. J. Grimes, S. N. Giddings, F. Feddersen, C. M. Beall, C. Lee, M. V. Santander, K. A. Prather, Airborne transmission pathway for coastal water pollution, PeerJ, 9 (2021) 1–19. https://doi.org/10.7717/peerj.11358

[20] S. Sharma, A. Bhattacharya, Drinking water contamination and treatment techniques, Appl. Water Sci., 7 (2017) 1043–1067. https://doi.

org/10.1007/s13201-016-0455-7

[21] O.Y.A. Costa, J. M. Raaijmakers, E. E. Kuramae, Microbial extracellular polymeric substances: Ecological function and impact on soil aggregation, Front. Microbiol., 9 (2018) 1–14. https://doi.org/10.3389/fmicb.2018.01636

[22] S. Herrera López, M. D. Hernando, M. J. Gómez, J. Santiago-Morales, R. Rosal, A. R. Fernández-Alba, Investigation of Galaxolide degradation products generated under oxidative and irradiation processes by liquid chromatography/hybrid quadrupole time-of-flight mass spectrometry and comprehensive two-dimensional gas chromatography/time-of-flight mass spectrometry, Rapid Commun., 27 (2013) 1237–1250. https://doi.org/10.1002/rcm.6575

[23] M. Celeiro, J. P. Lamas, M. Vila, C. Garcia-Jares, V. Homem, N. Ratola, T. Dagnac, M. Llompart, Determination of multiclass personal care products in continental waters by solid-phase microextraction followed by gas chromatography-tandem mass spectrometry, J. Chromatogr. A, 1607 (2019) 460398. https://doi.org/10.1016/j.chroma.2019.460398

[24] B. D. Su, C. Z. Min, C. D. Hui, The Determination of Galaxolide in water samples with SPME coupled with GC-MS, Adv. Mater. Res., 183 (2011) 184–187. https://doi.org/10.4028/www.scientific.net/AMR.183-185.184

[25] A. Sokol, A. Ratkiewicz, I. Tomaszewska, J. Karpinska, Kinetics and mechanistic studies of photochemical and oxidative stability of galaxolide, Water, 13 (2021) 1813. https://doi.org/10.3390/w13131813

[26] J. C. Lindon, G. E. Tranter, D. Koppenaal, Encyclopedia of spectroscopy and spectrometry, Academic Press, (2016). https://www.amazon.ca/-/fr/John-C-Lindon/dp/0128032243

[27] J. Rakhtshah, H. Shirkhanloo, N. A. Esmaeili, Rapid extraction of toxic styrene from water and wastewater samples based on hydroxyethyl methylimidazolium tetrafluoroborate immobilized on MWCNTs by ultra-assisted dispersive cyclic conjugation-micro-solid phase extraction, Microchem. J., 170 (2021) 106759. https://doi.org/10.1016/j.microc.2021.106759

[28] S. Teimoori, A.H. Hassani, New extraction of toluene from water samples based on nano-carbon structure before determination by gas chromatography, Int. J. Environ. Sci. Technol., 20 (2023) 6589–6608. https://doi.org/10.1007/s13762-023-04906-9

[29] B. Darpo, T. Nebout, P. T. Sager, Clinical evaluation of QT/QTc prolongation and proarrhythmic potential for nonantiarrhythmic drugs: The international conference on harmonization of technical requirements for registration of pharmaceuticals for human use E14 guideline, J. Clin. Pharmacol., 46 (2006) 498–507. https://doi.org/10.1177/0091270006286436

[30] USP 30 The United States Pharmacopeia 30th ed. (United States Pharmacopeial Convention: Rockville, 2007. https://www.usp.org/

[31] ASTM Standard Practice for Validation of Empirically Derived Multivariate Calibrations Methods, Document E2617–17, West Conshohocken, USA, 2018. https://standards.globalspec.com/std/4384102/astm-e2617-17

[32] V. Diwan, C. Stålsby Lundborg, A. J. Tamhankar, Seasonal and temporal variation in release of antibiotics in hospital wastewater: estimation using continuous and grab sampling, PLOS One, 8 (2013) e68715. https://doi.org/10.1371/journal.pone.0068715

[33] A. M. Gilmore, L. Chen, Optical early warning detection of aromatic hydrocarbons in drinking water sources with absorbance, transmission and fluorescence excitation-emission mapping (A-TEEM) instrument technology, In Next-Generation Spectroscopic Technologies XII, SPIE publisher, 10983 (2019) 45–52. https://doi.

org/10.1117/12.2522498

[34] S. M. Clegg, E. Sklute, M. D. Dyar, J. E. Barefield, R. C. Wiens, Multivariate analysis of remote laser-induced breakdown spectroscopy spectra using partial least squares, principal component analysis, and related techniques, Spectrochim. Acta B At. Spectrosc., 64 (2009) 79–88. https://doi.org/10.1016/j.sab.2008.10.045

[35] E. R. Ziegel, Handbook of Chemometrics and Qualimetrics, Part B, Technometrics, 42 (2000) 218-219. https://doi.org/10.1080/00401706.2000.10486023

[36] N. Altman, M. Krzywinski, P values and the search for significance, Nat. Methods, 14 (2017) 3–4. https://doi.org/10.1038/nmeth.4120

[37] D. Steiner, R. Krska, A. Malachová, I. Taschl, M. Sulyok, Evaluation of matrix effects and extraction efficiencies of LC–MS/MS methods as the essential part for proper validation of multiclass contaminants in complex feed, J. Agric. Food Chem., 68 (2020) 3868–3880. https://doi.org/10.1021/acs.jafc.9b07706

[38] A. Fajgelj, A. Ambrus, Guidelines for single-laboratory validation of analytical methods for trace-level concentrations of organic chemicals, In Principles and practices of method validation, pages179–252, 2000. https://doi.org/10.1039/9781847551757-00179

[39] S. Singh, N. Sharma, N. Kanojia, G. Kaur, S. Arora, Development and validation of UV-spectrophotometer method for analysis of fluvastatin sodium in polyethylene glycol 6000 and polyvinyl pyrollidone K-30 solid dispersions, Plant Arch., 20 (2020) 3365–3371. https://www.plantarchives.org/

[40] T. N. Rao, Validation of analytical methods, Calibration and validation of analytical methods- A sampling of current approaches, book publisher: Intech Open, 25 (2018) 131–41. http://dx.doi.org/10.5772/intechopen.72087